An Extra Galactic Dark Matter Flux and Its Expected Consequences

Seiterle, Felix-Alexander

January 4, 2022

Technical University Munich

Department of Physics

Dense and Strange Hadronic Matter

Prof. Dr. Laura Fabbietti

Supervisor

Prof. Dr. Laura Fabbietti
M.Sc. Stephan Königstorfer

Contents

List of Figures

1 Abstract

The following thesis assumes an extra galactic dark matter flux at Earth's position which equates to ~ 12 % of galactic dark matter measurements [2]. Recently a certain amount of dark matter has been proposed to be loose and homogeneously distributed within the Virgo Supercluster including the Local Group, and flowing through our galaxy [2]. In contrast to galactic dark matter solely located in Milky Way's dark matter halo, extra galactic dark matter particles need to be faster than the Milky Way's escape velocity of $\sim 600\,\mathrm{km/sec}$ [2].
As dark matter qualifies as an exotic source for antimatter in cosmic rays and as such can be indirectly proven through antimatter measurements [3] an extra galactic dark matter flux implies significant consequences. In fact, the source term of created antimatter is possibly affected by dark matter density, the cross section $< \sigma v >$ and the produced spectrum of antinuclei. To be more specific, the change of speed calculated for the extra galactic dark matter being at the exact speed of Milky Way's escape velocity affects both the cross section and the produced spectrum of antinuclei while the sole existence of extra galactic dark matter impacts the antinuclei source term proportional to the square of dark matter density.
However, the effect on the cross section is negligible because s-wave annihilation is velocity independent and it dominates p-wave annihilation by ~ 6 orders. The effect on the produced spectrum of antinuclei is determined to a maximum value of ~ 1.4 % and therefore negligible as well.
To zeroth order the dark matter density of extra galactic dark matter is suggested to be homogeneously distributed throughout the Milky Way. A shifted Navarro-Frenk-White profile is proposed accordingly. Exhausting Milky Way's rotation curve it is tried to determine the corresponding constants of the shifted Navarro-Frenk-White profile by applying Gauss's law for gravity. It is recognized that neither Gauss's law for gravity is applicable on the shifted Navarro-Frenk-White profile nor is Milky Way's rotation curve affected by any constant matter distribution as is the case for extra galactic dark matter.
Applying most basic principles a two-dimensional simulation is set up that models the Milky Way's function as a lens for extra galactic dark matter. The lensing effect causes extra galactic dark matter density to no longer be constant: within one direction it increases by ~ 100 % at Earth's position. It is explained that due to the lensing effect the measurement of dark matter from Milky Way's rotation curve needs to be reevaluated as it accounts for galactic and extra galactic dark matter. Furthermore, the galactic dark matter density determined from Milky Way's rotation curve does no longer hold. Means for further research are provided.

2 Introduction

Our universe is 13.8 billion years old [4]. It is assumed to consist of $\sim 5\%$ ordinary baryonic matter, $\sim 26\%$ dark matter, and $\sim 69\%$ dark energy [5]. However, no dark matter particle has been directly detected so far [4]. The strongest indication for dark matter is found in the orbital velocities of the stars of our galaxy. Such distributions are called rotation curves. By definition, a rotation curve is the mean circular velocity around a nucleus as a single function of radius [1]. For circular motion Newtonian physics derives that particles' orbiting speed decreases with increasing radius [6]. As Milky Way's mass distribution is not point-like Newtonian physics can not be applied. As a matter of fact, Gauss's law for gravity (see equation 6) proves that the gravitational force exhibits identically when applied on the same volume and differently distributed mass density [6]. Thus, one might assume luminous matter to be delta distributed and hence point-like as long as rotation curves beyond the border of luminous matter are investigated. In contrast to a Keplerian speed distribution rotation curves show a flat behaviour up to a factor of $\sim 10\,\mathrm{kpc}$ exceeding luminous matter [6, 7]. This contradiction is solved by proposing additional unseen matter: dark matter [5]. In 1933, the existence of dark matter was already suggested by Zwicky et al. Zwicky explains velocity disparities between experiment and theory in his work on the Coma cluster of galaxies [8, 9]. The existence of dark matter is further supported by gravitational lensing effects, fluctuations in the cosmic microwave background and more [5, 8].
Generally ordinary baryonic matter and luminous matter are used interchangeably in this context: the latter being the opposite of dark matter which does not interact with electromagnetic forces and is not observable in telescopes. As dark matter has not been detected so far research has been difficult and is categorized into direct methods, indirect methods, and production at high-energy colliders like the one at CERN [4]. Likewise to dark matter's indiscernibility from telescopes, no signal can be detected in collider settings. Researchers look for missing masses in experiments along a trace of familiar particles such as gluons, Z-bosons, photons and quarks [4]. Direct methods look for small scattering signals between a dark matter particle and an atomic nucleus [4]. To detect such a signal, background noise from natural radioactivity has to be accordingly low, as is the case for experiments conducted deep underground [4]. Indirect methods search for antinuclei, amongst other things [4]. It is believed that dark matter particles annihilate each other, producing matter and antimatter. Antinuclei at low energy are the promising candidate as their signal exceeds background noise from astrophysical sources by several orders [10]. In contrast, possible signals of dark matter annihilation at high energy are more difficult to

distinguish from background noise as they can also originate from cosmic ray collisions [11]. The signal of dark matter annihilation into ordinary matter is even harder if not impossible to discern due to the vast prevalence of ordinary matter in the universe.
Dark matter is prevailingly assumed to embed galaxies, galaxy groups, and galaxy clusters in so called dark matter halos without any exchange between them [2, 9, 12, 13]. Hence, in most models only the dark matter bound in galaxy's halos is considered; however, an extragalactic dark matter component might exist. Recent research proposed some dark matter to be loose and homogeneously distributed within the Virgo Supercluster including the Local Group streaming throughout the Milky Way [2]. Calculations define its density to be 12 % of currently measured dark matter at Earth's position [2]. Consequently, the dark matter distribution and the spectrum of antimatter production are subject to change. This is of extreme importance as the antinuclei source term is proportional to the square of dark matter density and as such strongly impacts the indirect method. For this reason chapter 3 "Assumptions and Theory" discusses the status quo and chapter 4 "An Extra Galactic Dark Matter Flux" introduces the extra galactic dark matter.

3 Assumptions and Theory

3.1 Basics of Astronomy

Our universe is hierarchically structured into different regions of density [14]. The greatest entities are so called superclusters like the Virgo Supercluster and are defined as a collection of at least two clusters [14]. The Virgo Supercluster encloses a domain of $\sim 40\,\mathrm{Mpc}$ [15], containing the Local Group in its outskirts [14]. Three requirements must be fulfilled in order for galaxies to belong to the Local Group:

a) the distance of the galaxy should be $\lesssim 1.5\,\mathrm{Mpc}$;

b) mean radial velocity and solar apex distance relations should be close to the ones of established group members;

c) and the galaxy should not be linked to any group of galaxies known to be outside the limits of the Local Group [16].

The distance between the known members of the Local Group, Andromeda galaxy and Milky Way, is $\sim 750\,\mathrm{kpc}$ [2]. The latter is often modelled as a cylinder with a radius of $\sim 20\,\mathrm{kpc}$ [17]. Finally, the Earth's position within the Milky Way is assessed to fall between $7.5\,\mathrm{kpc}$ to $8.5\,\mathrm{kpc}$ [1]. In this thesis, it is set to $8.0\,\mathrm{kpc}$.

3.2 A Short Overview of Dark Matter

As has been broadly described in the introduction dark matter's existence is still not ensured. Hence, there are different theories on its nature. They are categorized in hot and cold dark matter theories characterising relativistic and non-relativistic speeds [18]. Neutrinos are electromagnetically neutral and extremely light, ideally matching the former category [4, 18]. Probably the most associated example of the latter are weakly interacting massive particles, the so called WIMPs [4]. Hot dark matter theories involve dark matter particles to form clusters which will later fall apart into galaxies [4]. In comparison, cold dark matter theories suggest a decoupling of dark matter particles from hot plasma in the early universe allowing galaxies to gradually form and accumulate into clusters [4]. Moreover, cold dark matter theories align with the idea of likening the universe to an ideal gas which cools down due to expansion. Independently from the chosen theory dark matter should be stable over billion of years and very likely collisionless [18].
The following thesis considers only WIMPs. Constraints of the annihilation cross section and measurements conducted by AMS-02 assessed the mass to range between $50\,\mathrm{GeV}$ to $1000\,\mathrm{GeV}$ [10, 19]. Additionally, most recent data propose the candidate range for WIMP mass between $40\,\mathrm{GeV}$ to $130\,\mathrm{GeV}$ [3, 10].

3.3 The Source Function of Antinuclei from Dark Matter Annihilation

According to current knowledge there are four possible sources of antinuclei [20]. These are cosmic rays' spallation on the interstellar medium, supernova remnants, the evaporation of primordial black holes, and dark matter annihilation [20]. After their creation process, antinuclei propagate through the universe and are affected by diffusion, convection and electromagnetic and hadronic interactions during which they can fragment, decay or annihilate [21]. Therefore, a function describing antinuclei can be split into three basic terms:

a) source,

b) propagation,

c) and destruction [21].

Focusing on the source function, dark matter's share is defined by [22]

$$Q(\vec{r}, T) = \frac{1}{2} \frac{\rho_\chi^2(\vec{r})}{m_\chi^2} < \sigma v > \frac{dN}{dT}. \tag{1}$$

Q is the created antimatter per unit volume per unit time per unit kinetic energy, ρ_χ is the dark matter density, m_χ is the dark matter mass, $< \sigma v >$ is the thermally-averaged zero-temperature cross section, and $\frac{dN}{dT}$ is the so called injection spectrum. The injection spectrum is the produced spectrum of antinuclei normalized to a single dark matter annihilation with T being the kinetic energy [23].
Common dark matter density distribution models are the Navarro-Frenk-White profile, the Einasto profile, and the isothermal profile [24]. This thesis solely focuses on the Navarro-Frenk-White profile.
To better categorize annihilation effects, the cross-section is usually expanded to[1] [25]:

$$< \sigma v > = a + b \cdot v^2 + O(v^4). \tag{2}$$

- The first term a represents s-wave annihilation [25].
- The second term $b \cdot v^2$ represents p-wave annihilation [25].

However, this expansion is only valid for dark matter at non-relativistic speeds [26] as is the case for cold dark matter, especially WIMPs.

Summing up everything, the equation works like this: The dark matter distribution divided by the dark matter mass delivers the number density of interacting dark matter particles. In return, the interaction scale of these dark matter particles is given by the cross section. Finally, the actual differential number of produced antimatter over a differential kinetic energy is given by the injection spectrum.

3.4 Milky Way's Rotation Curve

3.4.1 Calculating Rotational Velocity

As explained in the introduction dark matter's existence was discovered in rotation curves. To determine the dark matter distribution in the Milky Way, its rotation curve is studied. Usually the Milky Way is separated into five divisions, namely:

a) a central black hole (see figure 1),

b) an inner exponential-spherical bulge (see figure 2),

c) an outer exponential-spherical bulge (see figure 4)

d) an exponential flat disk (see figure 6),

e) a dark matter halo (see figure 7) [1] .

After discussing some general effects for all divisions each one is described individually. Each component creates its own gravitational potential Ψ_i [27]. Thus, each component exerts its own force and is as such partially responsible for the stars' rotational velocity V [27]. By using a superposition of these gravitational potentials, the Milky Way's rotation curve is expressed as follows [1]:

$$V = \sqrt{\sum_i r \cdot \frac{d\Psi_i}{dr}}. \tag{3}$$

Therefore, rotational velocities from different parts displayed in the rotation curve are added in quadrature. As the gravitational force is a conservative force, each division's gravitational field $\mathbf{g}_i$ can be expressed by its particular scalar potential Ψ_i,

$$\nabla \Psi_i = -\mathbf{g}_i. \tag{4}$$

Taking advantage of spherical coordinates and gravitational field's radial symmetry, equation 4 simplifies to

$$\nabla \Psi_i = \frac{\partial \Psi_i}{\partial r} = -|\mathbf{g}_i|. \tag{5}$$

[1] Natural units applied with v being the speed as a fraction of c.

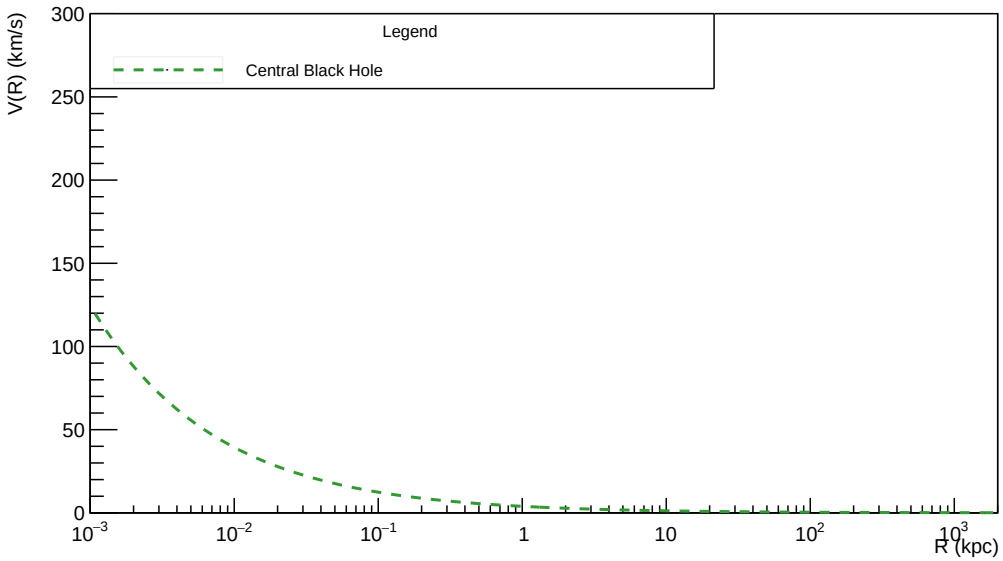

Figure 1: Partial rotational velocity caused by Milky Way's central black hole

Applying the Gauss's law for gravity, the gravitational field can be extracted [1, 27], see equation 6. The Gauss's law for gravity works analogous to the Gaussian Law for electrodynamics [6]. Utilizing this law, however, means gravitational forces outside the chosen volume are not taken into account and need to either add up to zero or be negligible. Like before ρ is the mass distribution and G is the gravitational constant [6]

$$\nabla \mathbf{g} = -4\pi G \cdot \rho. \tag{6}$$

The integral form of Gauss's law for gravity is written as follows [6],

$$\oint_{\partial V} \mathbf{g} \cdot \mathbf{dA} = -4\pi G \cdot M. \tag{7}$$

M is the integrated mass from the mass distribution. For spherical symmetries ∂V is the surface of a sphere and equation 7 becomes trivial,

$$-|\mathbf{g}| = \frac{G \cdot M}{r^2}. \tag{8}$$

Inserting equation 8 into equation 3, a single division causes a rotational velocity

$$V_i = \sqrt{\frac{G \cdot M}{r}}. \tag{9}$$

To sum it up, rotation curves can also be expressed by mass, as long as the constraints mentioned above hold.

3.4.2 A Central Black Hole

In Milky Way's center a super massive black hole is located, called Sagittarius A* [28]. Its mass M_{BH} is estimated to be $3.6 \times 10^6\,\mathrm{M}_\odot$ [1]. The black hole is considered to be a point mass at the nucleus exerting a spherically symmetric force [27]. Therefore, equation 9 can be utilized:

$$V = \sqrt{\frac{G \cdot M_{BH}}{r}}. \tag{10}$$

A representation of Sagittarius A*'s caused rotational velocity is provided in figure 1. At distances greater than 1 kpc the black hole's influence becomes negligible which is owed to its position at 0 kpc and $V \sim r^{-\frac{1}{2}}$.

3.4.3 An Inner and Outer Exponential-Spherical Bulge

The classical bulge is separated into the inner and outer bulge [29]. The inner bulge is an accumulation of very old stars ($>$ 10 billion years) [30]. It spans from the galactic center to $\sim$ 3 kpc [30]. For both divisions the induced circular rotational velocity is calculated by

$$V = \sqrt{\frac{G \cdot M_B}{r} \cdot F\left(\frac{r}{a}\right)} \tag{11}$$

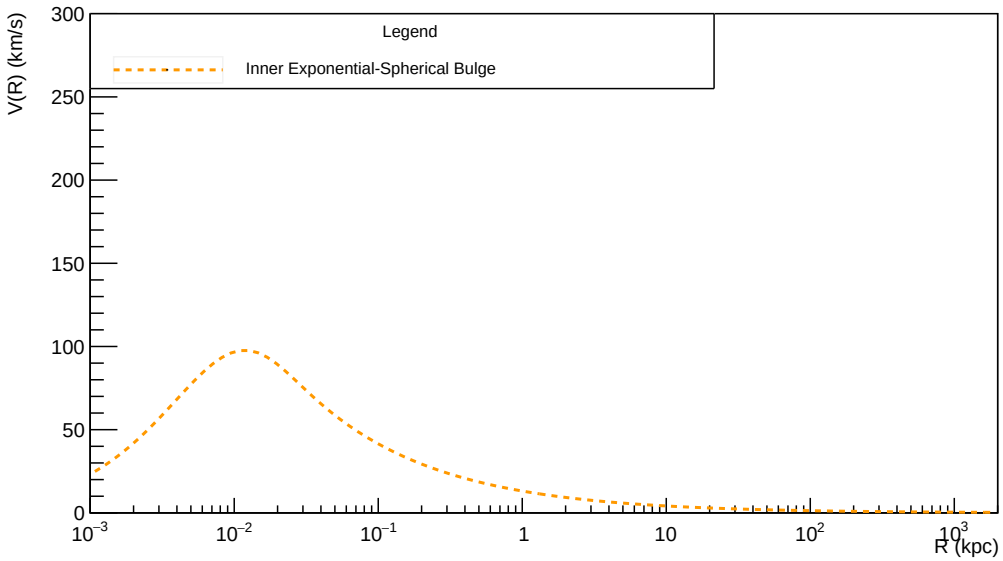

Figure 2: Partial rotational velocity caused by Milky Way's inner exponential-spherical bulge

with

$$F(x) = 1 - e^{-x}(1 + x + \frac{x^2}{2}) \tag{12}$$

where $x = r/a$. The mass M_B for inner and outer bulge are determined at $(0.4 \pm 0.1) \times 10^8\,\mathrm{M}_\odot$ and $(0.92 \pm 0.02) \times 10^{10}\,\mathrm{M}_\odot$ respectively [29]. Lowercase a is the scale factor and found to be $(0.0035 \pm 0.0004)\,\mathrm{kpc}$ and $(0.120 \pm 0.003)\,\mathrm{kpc}$ for the inner and outer bulge respectively [1].

Figure 3 and 5 depict the mass density distribution of the inner and outer exponential-spherical bulge. Figure 2 and 4 show the induced rotational velocity of the inner and outer exponential-spherical bulge. In accordance with maxima from Milky Way's rotation curve the inner bulge's partial rotational velocity peaks at $\sim 0.01\,\mathrm{kpc}$ and the outer one's at $\sim 0.5\,\mathrm{kpc}$ [1]. Especially by comparing these peaks and their substantial contribution regions to Milky Way's rotation curve 9, the division of the Milky Way into separated parts becomes reasonable. For example, the inner exponential-spherical bulge's caused partial rotational velocity rises til its maxima, filling up missing rotation curve velocities created from other components, and vanishes as the outer exponential-spherical bulge's induced partial rotational velocity grows.

3.4.4 An Exponential Flat Disk

In the method laid out in paper [1] the disk is considered one whole[2]. The disk's induced rotational velocity is calculated by [1]

$$V = \sqrt{\frac{\pi G \cdot \Sigma_0 \cdot r^2 \left(K_0 I_0 - K_1 I_1\right)}{R_d}} \tag{13}$$

where Σ_0 is the total average mass density, R_d is the scale factor and K_i and I_i are the modified Bessel functions. The total average mass density is expressed through the disk mass M_{disk} by

$$\Sigma_0 = \frac{M_{disk}}{2\pi \cdot R_d^2}. \tag{14}$$

The disk mass and scale factor respectively are determined as $(0.9 \pm 0.1) \times 10^{11}\,\mathrm{M}_\odot$ and $(4.9 \pm 0.4)\,\mathrm{kpc}$ [1].

The caused rotational velocity by Milky Way's exponential flat disk is depicted in figure 6. At $\sim 10\,\mathrm{kpc}$ the contribution to the rotation curve from the exponential flat disc reaches its maximum at $\sim 175\,\mathrm{km\,s^{-1}}$.

[2] In some literature [31–33] and paper [34] the disk is separated further into a thin and a thick disk. Milky Way's rotation curve shows 3 maxima. The first two are covered by the inner and outer exponential-spherical bulge while the 3rd one of the disk coincides with the maxima of the dark matter halo. Therefore, deriving further detail from the rotation curve like the separation of the disk is difficult.

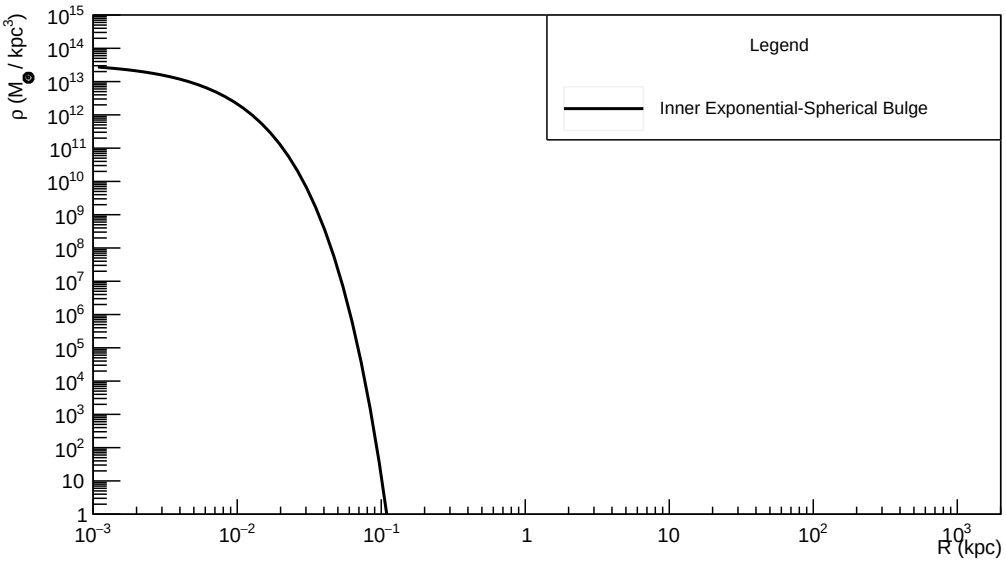

Figure 3: Mass density distribution of Milky Way's inner exponential-spherical bulge

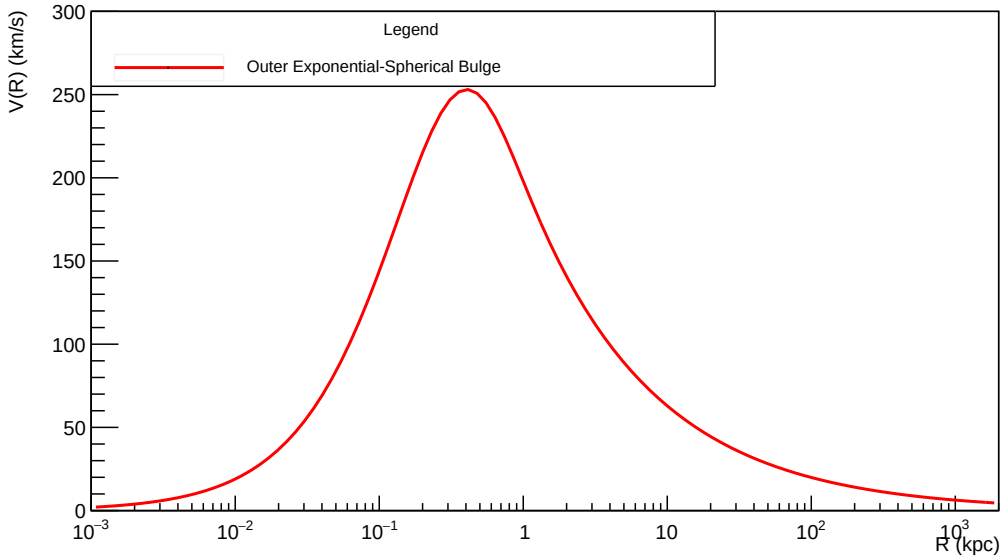

Figure 4: Partial rotational velocity caused by Milky Way's outer exponential-spherical bulge

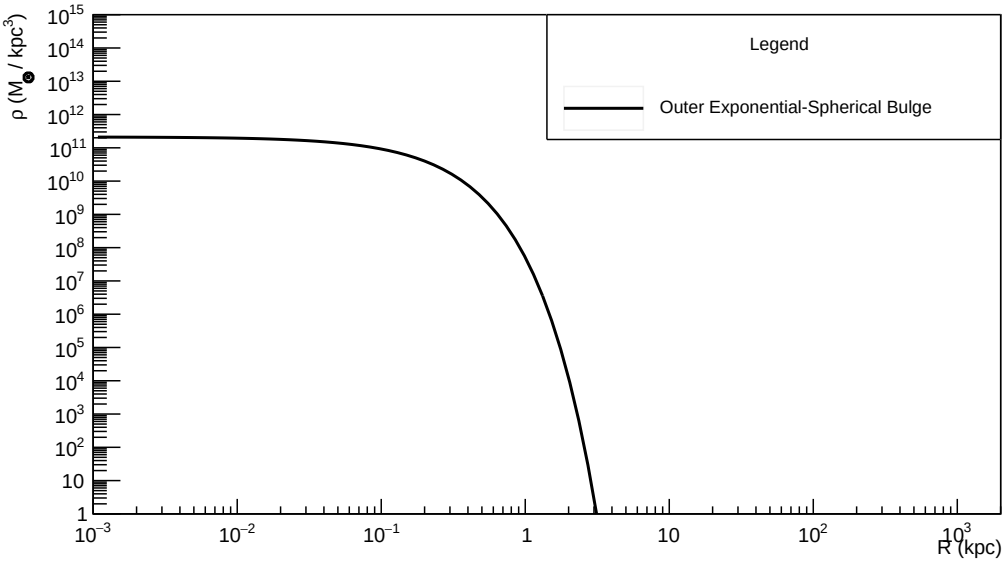

Figure 5: Mass density distribution of Milky Way's outer exponential-spherical bulge

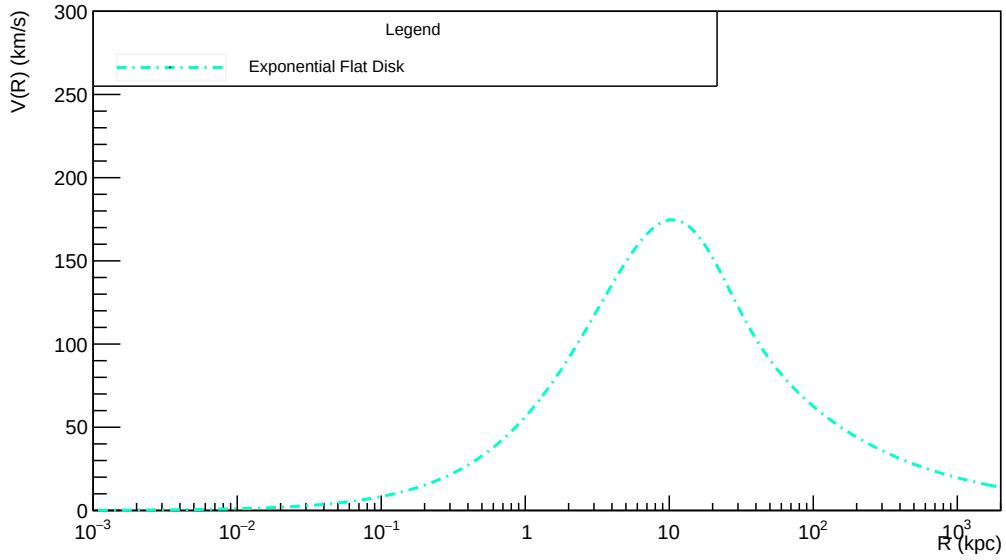

Figure 6: Partial rotational velocity caused by Milky Way's exponential flat disk

3.4.5 A Dark Matter Halo

The dark matter halo is characterized by its density distribution, the Navarro-Frenk-White profile:

$$\rho_\chi = \frac{\rho_0}{r/r_s[1+(r/r_s)]^2}, \tag{15}$$

where r is the radius measured from the galaxy center, ρ_0 is the characteristic density and r_s is the scale factor. For obvious reasons experiments are comparatively easily conducted on and nearby the Earth which is why the most precise data measured from Earth is utilized to extract function values. Hence characteristic density and scale factor are fitted accordingly. However, the results of earth-near experiments also have their limitations, as it is significantly more difficult to determine the Milky Ways' structure and kinematics compared to other galaxies since we are part of the Milky Way [35].

Dark matter is assumed to be spherically symmetric distributed throughout the Milky Way. Thus, one can follow the instructions in section 3.4.1 in order to apply equation 9. It is salient to ensure that the integrated sphere has to be sufficiently large to comprise all dark matter particles of the Navarro-Frenk-White profile. In

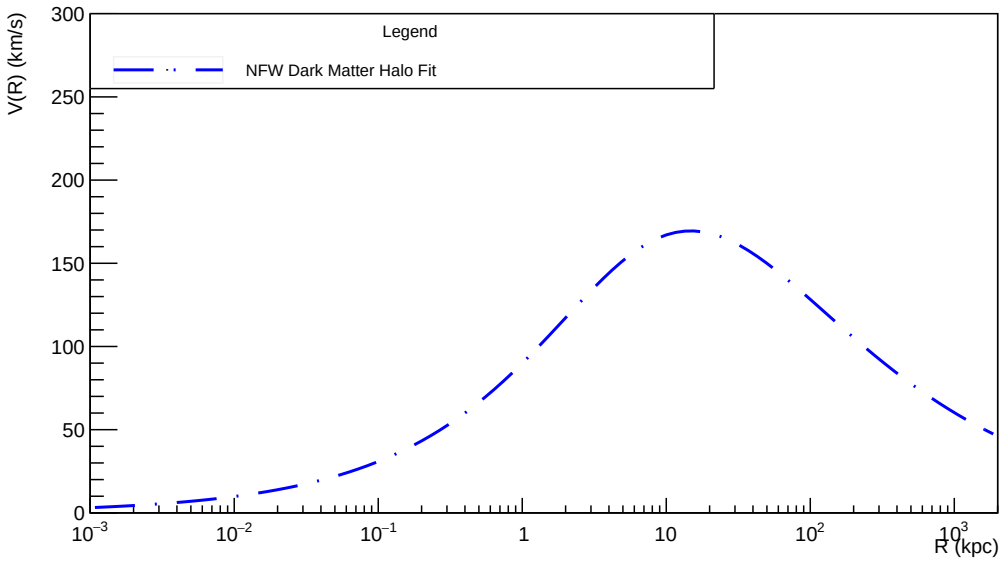

Figure 7: Partial rotational velocity caused by Milky Way's dark matter halo

order to do so the utilized upper integration limit R equals 100 kpc for the following calculations and one obtains

$$V = \sqrt{\frac{G \cdot M_{DM}}{r}} \tag{16}$$

with a dark matter's mass M_{DM} of

$$\begin{aligned} M_{DM} &= 4\pi \left(\rho_0 \cdot r_\mathrm{s}^3 \left(\ln\left(|r + r_\mathrm{s}|\right) + \frac{r_\mathrm{s}}{r + r_\mathrm{s}} \right) \right) \Bigg|_0^R \\ &= 4\pi \left(\rho_0 \cdot r_\mathrm{s}^3 \left(\ln\left(|R + r_\mathrm{s}|\right) \right) + \frac{r_\mathrm{s}}{r_\mathrm{s} + R} \right) \\ &\quad - 4\pi \left(\rho_0 \cdot r_\mathrm{s}^3 \left(\ln\left(|r_\mathrm{s}|\right) + 1 \right) \right). \end{aligned} \tag{17}$$

In figure 7 characteristic density and scale factor are fitted to $5.3 \times 10^7\,\mathrm{M}_\odot\,\mathrm{kpc}^{-3}$ and 6.83 kpc respectively, showing the caused rotational velocity by Milky Way's dark matter halo. Figure 8 shows a Navarro-Frenk-White profile with said fit values and compares it to a further Navarro-Frenk-White profile from paper [1]. In the latter characteristic density and scale factor are set to $(2.90 \pm 0.30) \times 10^7\,\mathrm{M}_\odot\,\mathrm{kpc}^{-3}$ and (10.0 ± 0.5) kpc. Evidently the self-made fit deviates from the paper, but in linear scales' comparison the deviation is acceptable. This might be due to differently chosen integration limits, the utilization of Gaussian's Law for mass, a coding error, a different fit program or any combination of these factors.

3.4.6 Illustration

Figure 9 features all five components including Milky Way's rotation curve and its data points. The fitted rotation curve and data points align very well until $\sim 10 \times 10^3$ kpc, χ^2_{57} equals to be 7.472 822 with the lower index of 57 denoting the degree of freedom. Rotation curve and data points would possibly still coincide with each other if measurements carried out at such large distances were not as uncertain. Additionally, new effects may arise accounting for these large deviations as Milky Way ceases at ~ 20 kpc.

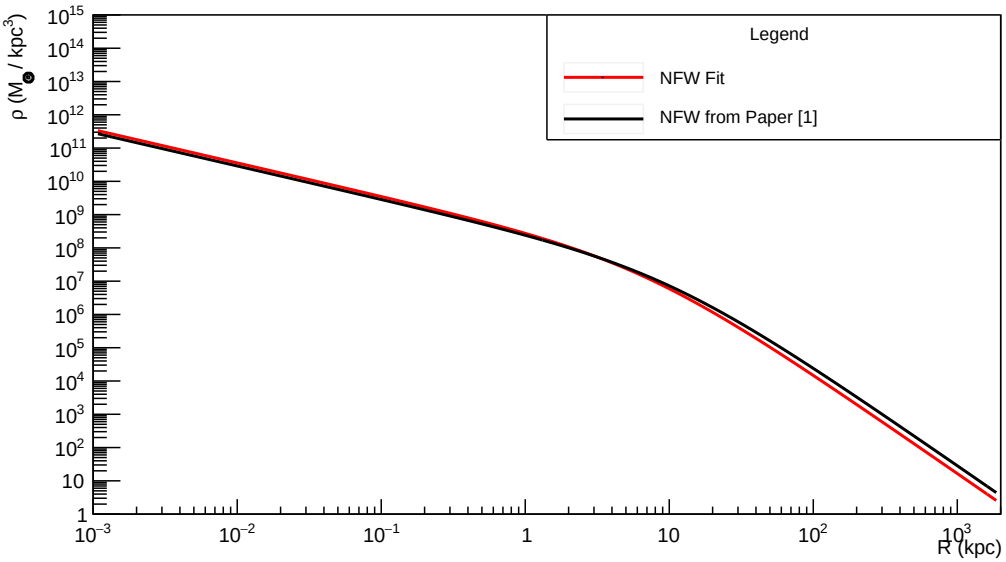

Figure 8: Mass density distribution of fitted Navarro-Frenk-White profile and Navarro-Frenk-White profile from [1], the first one with integrated dark matter distribution.

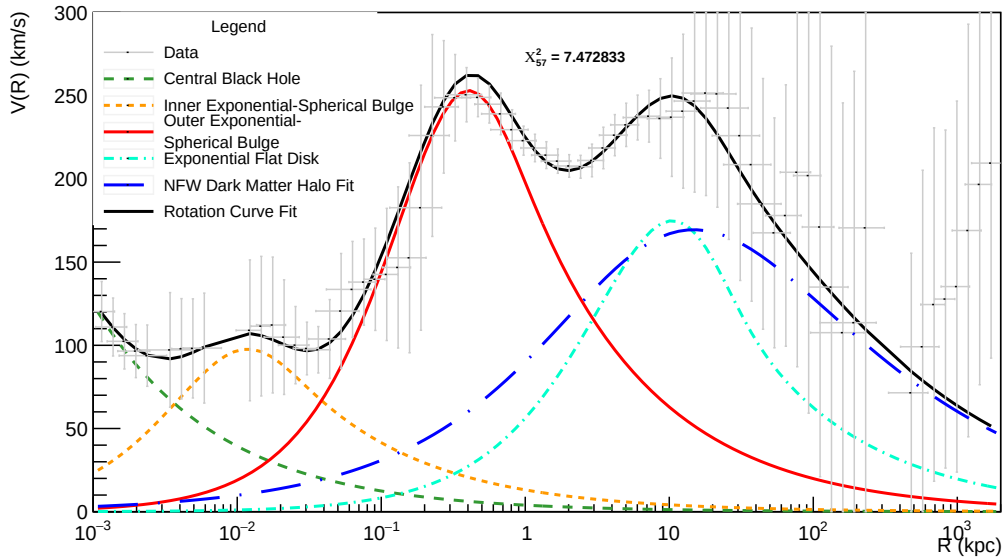

Figure 9: Milky Way's rotation curve fit with $\chi^2_{57} = 7.472822$ including data points and all components, namely: a central black hole, an inner exponential-spherical bulge, an outer exponential-spherical bulge, an exponential flat disk, a dark matter halo fit from the Navarro-Frenk-White profile

3.5 Kinetic Energy and Reference Frame Transformation

Kinetic energy is not lorentz invariant and thus depends on the reference frame. Consequently the differential injection spectrum from equation 1 depends on it as well. Assuming galactic dark matter to be moving at non-relativistic speed with respect to the Milky Way's reference frame, the differential injection spectrum is measured from our galaxy's reference frame. Hence these two reference frames are almost identical and the difference between them can be neglected: center of mass frame and laboratory frame are the same. For an extra galactic dark matter flux relativistic speeds are considered and the simplification is challenged. Therefore, a short review on reference frame transformation is supplied here.
In special relativity it is necessary to describe the particle's total energy E as the sum of rest mass m_0 and kinetic energy T in relation to the used reference frame. Applying natural units this relation is expressed as

$$E = m_0 + T \ . \tag{18}$$

The actual reference frame shift can be conducted by using the following formula[3] [36]:

$$\begin{pmatrix} E' \\ p' \end{pmatrix} = \begin{pmatrix} \gamma & -\beta\gamma \\ -\beta\gamma & \gamma \end{pmatrix} \begin{pmatrix} E \\ p \end{pmatrix} \tag{19}$$

where p is the momentum, γ the Lorentz factor, and primed quantities represent their shifted value. The momentum can be substituted by[4]

$$p = \sqrt{m_0^4 - E^2}. \tag{20}$$

As the mass of a specific antinuclei equals the same ordinary nuclei's mass the rest mass is usually known. Thus, the kinetic energy can be calculated for each reference frame solely from its velocity:

$$T' = \gamma \left((m_0 + T) - \beta \left(\sqrt{m_0^4 - (m_0 + T)^2} \right) \right) - m_0. \tag{21}$$

To finally calculate the transformed differential injection spectrum the following trick is applied:

$$\frac{dN}{dT'} = \frac{dT}{dT'} \frac{dN}{dT}. \tag{22}$$

The conversion factor $\frac{dT}{dT'}$ equals to

$$\frac{dT}{dT'} = \gamma \left(\frac{\beta \left(T' + m_0 \right)}{\sqrt{m_0^4 - \left(T' + m_0 \right)^2}} + 1 \right), \tag{23}$$

and final results are presented in chapter 4.3.

4 An Extra Galactic Dark Matter Flux

4.1 A Modified Dark Matter Distribution

Latest research proposes dark matter to be drifting homogeneously and unbound within the Local Group and the Virgo Supercluster and streaming through the Milky Way [2]. At Earth's position its density is calculated to equal $\sim 3.7 \times 10^{-2}\,\mathrm{GeV/cm^3}$ which equates to ~ 12 % of current galactic dark matter measurements. It is noticed that due to the different scales a homogeneous distribution within the Local Group does not imply a constant density within the Milky Way per se in spite of the following assumption:
to zeroth order, the extra galactic dark matter is assumed to be constant within the Milky Way. Accordingly, a new dark matter distribution could look like a shifted Navarro-Frenk-White profile:

$$\rho_\chi = \frac{\rho_0}{r/r_s[1 + (r/r_s)]^2} + \rho_{\chi_{ex}}, \tag{24}$$

where $\rho_{\chi_{ex}}$ is the extra galactic dark matter density. Furthermore, galactic and extra galactic dark matter are assumed to be distributed spherically symmetric. Consequently, the same equations as in section 3.4.5 are applied:

$$V = \sqrt{\frac{G \cdot M_{\chi_{ex}}}{r}} \tag{25}$$

[3] Natural units are applied.
[4] Natural units are applied.

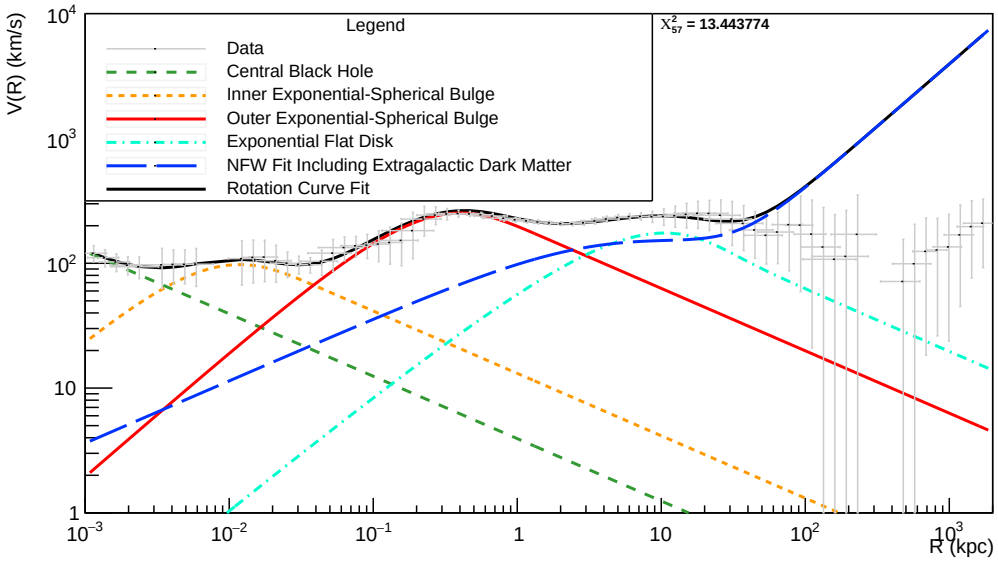

Figure 10: Milky Way's logarithmic rotation curve fit with $\chi^2_{57} = 13.443774$ including data points and all components, namely: a central black hole, an inner exponential-spherical bulge, an outer exponential-spherical bulge, an exponential flat disk, a dark matter halo fit from the shifted Navarro-Frank-White profile

and

$$\begin{aligned} M_{DMex} &= 4\pi \left(0.88\rho_0 \cdot r_s^3 \left(\ln\left(|r + r_s|\right) + \frac{r_s}{r + r_s} \right) + \frac{0.12\rho_0 \cdot r_s \cdot r^3}{3 \cdot 8kpc \left(\frac{8kpc}{r_s} + 1 \right)^2} \right) \Bigg|_0^R \\ &= 4\pi \left(0.88\rho_0 \cdot r_s^3 \left(\ln\left(|R + r_s|\right) + \frac{r_s}{R + r_s} \right) + \frac{0.12\rho_0 \cdot r_s \cdot R^3}{3 \cdot 8kpc \left(\frac{8kpc}{r_s} + 1 \right)^2} \right) \\ &\quad - 4\pi \left(0.88\rho_0 \cdot r_s^3 \left(\ln\left(|r_s|\right) + 1 \right) \right). \end{aligned} \tag{26}$$

To determine the characteristic density and scale factor of the shifted Navarro-Frenk-White profile the galactic and extra galactic dark matter coinciding with Milky Way's rotation curve measurements is deployed, especially for Earth's position. It is hence assumed that galactic and extra galactic dark matter density can linearly be added up to 100 %:

$$\rho_\chi(r = 8\ kpc) = \frac{0.88\rho_0}{r/r_s[1 + (r/r_s)]^2} + \frac{0.12\rho_0}{r/r_s[1 + (r/r_s)]^2}. \tag{27}$$

Characteristic density and scale factor are respectively fitted to $1.43 \times 10^8\ \mathrm{M}_\odot\ \mathrm{kpc}^{-3}$ and 3.83 kpc. Figure 10 depicts the resulting rotation curve in logarithmic scales, χ^2_{57} equals 13.443 774 with the lower index of 57 denoting the degree of freedom.

Clearly data points and rotation curve begin to deviate exceedingly from each other at ~ 40 kpc. The severely increasing caused rotational velocity from 40 kpc upward can also be seen in the according galactic dark matter halo and extra galactic dark matter flux, figure 11. The deviation Σ is quantified in figure 12 by using the following formula

$$\Sigma = \frac{f - v}{\sigma_D}, \tag{28}$$

where f is the fit, v is the data and σ_D is the standard deviation. Between 0.001 kpc to 100 kpc the error is contained below 1.5 Σ which denotes an acceptable result; however, further qualms arise by looking at the shifted Navarro-Frenk-White profile in figure 13.
From ~ 40 kpc upwards the shifted Navarro-Frenk-White profile remains constant. Assuming to be located in the middle of all dark matter, a net force of 0 N should be exerted due to the symmetric distribution canceling out all forces. As the gravitational force is inversely proportional to the square of radius, deviations of these

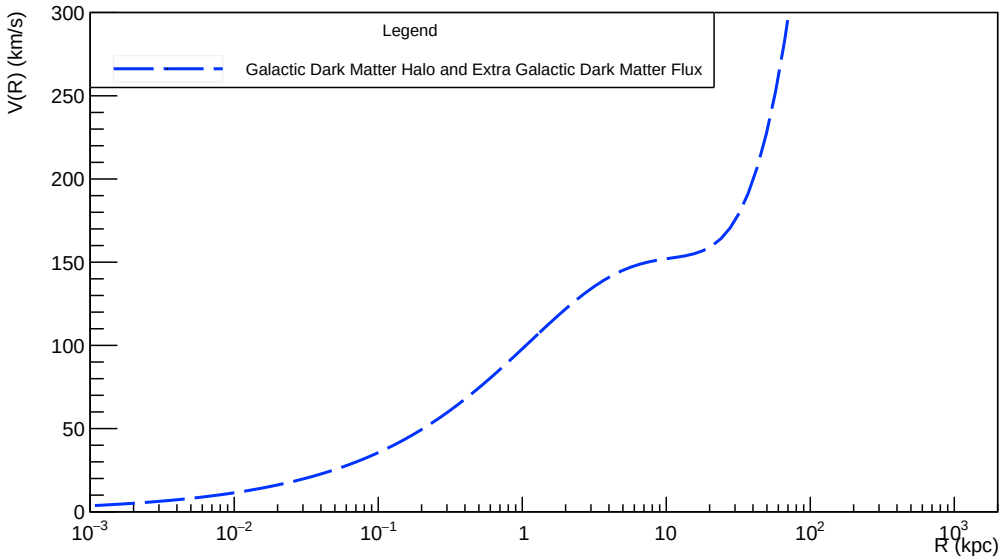

Figure 11: Partial rotational velocity caused by Milky Way's galactic dark matter halo and extra galactic dark matter flux

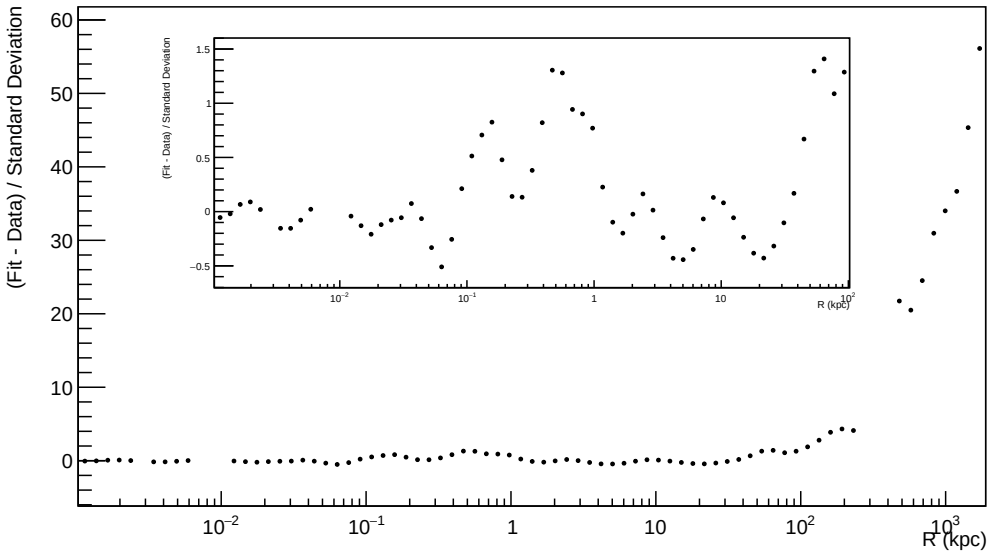

Figure 12: (Fit - Data) / Standard Deviation

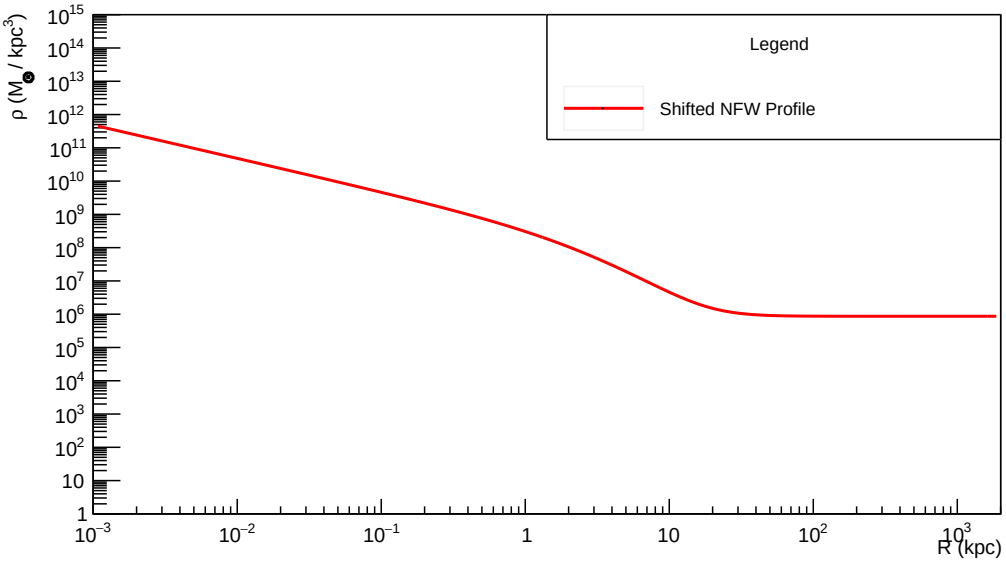

Figure 13: Mass density distribution of a shifted Navarro-Frenk-White profile

even distributions become negligible at large enough radii. Hence

$$\nabla\Phi \sim \mathbf{F} \sim \nabla\rho \tag{29}$$

applies and a constant dark matter flux should remain without effect on the rotation curve. Yet, the rotation curve shows a different picture which must be wrong. The constantly increasing velocity from 40 kpc upwards would imply a force responsible for the rise in velocity.
The failure is caused by utilizing the Gaussian Law. In contrast to the original Navarro-Frenk-White profile the shifted Navarro-Frenk-White profile does not slump to zero at any point. Thus, it is not possible to choose a volume large enough for the integration comprising all dark matter particles. Consequently gravitational forces exerted from particles outside the chosen volume are not taken into account and falsify the use of the Gaussian Law. In addition, the assumption of a spherically symmetric distribution of extra galactic dark matter is invalid as can be seen in figure 14 of the next chapter. Moreover, it is to be questioned whether the Gaussian Law is even applicable to the original spherically symmetric Navarro-Frenk-White profile as above reasoning (relation 29) and equation 8 contradict each other. To be more precise one may multiply both sides of equation 8 with the accelerated mass m and substitute dark matter mass M back to the integration of space over density:

$$|\mathbf{F}| = -\frac{G \cdot m}{r^2} \int_V d^3x \; \rho. \tag{30}$$

Clearly, this equation does not depend on $\nabla\rho$.
In spite of the errors explained it is discernible that from 0 kpc to 40 kpc the simplifications still enable an appropriate outcome. This, however, should be evaluated carefully as any impact of constant extra galactic dark matter on Milky Way's rotation curve is factually futile as stated previously. The fact that a constant shift of dark matter induces a difference on the production of antimatter still remains (see equation 1). Within the constraint that extra galactic dark matter does not interfere with Milky Way's rotation curve, the $\sim$ 12 % of extra galactic dark matter should simply be added on top of the measured galactic dark matter density derived from Milky Way's rotation curve in order to determine the new spectrum of antimatter production.

4.2 Gravitational Lensing Effect

Proceeding from above results one might consider the Milky Way to function as a lens for the extra galactic dark matter flux: the extra galactic dark matter particles are persistently pulled to the Milky Way's center by traversing the galaxy. Correspondingly, density varies with respect to its position and factually does affect the rotation curve. To make a first estimate of a possible lensing effect and its magnitude, a simulation is set up applying the following simplifications:

a) only an expanded dark matter distribution in x-direction moving in y-direction is taken into account;

b) galactic plane and Local Group's plane are aligned and the former is part of the latter;

c) the extra galactic dark matter particles, velocities and acting forces are within the plane.

In line with Newton's mechanics the following acceleration[5] a is utilized from the data of Milky Way's rotation curve:

$$a = \frac{V^2}{r}. \tag{31}$$

Starting at a distance of $\sim 200\,\mathrm{kpc}$ from the Milky Way's center 2000 extra galactic dark matter particles are simulated.
Figure 14 shows the density distribution of such a simulation in the Local Group's plane. As can be seen, the result depends on observing the distribution along a horizontal or vertical axis within the plane, figure 15 and 16 depict this respectively. The density deviation profile A is calculated by

$$A = \frac{\rho - \rho_N}{\rho_N}, \tag{32}$$

where ρ is the extra galactic dark matter distribution according to its position and ρ_N is the normalization factor, e.g. the extra galactic dark matter density distribution far beyond the Milky Way galaxy.
A huge lensing effect of $\sim$ 100 % is seen in figure 15, increasing the extra galactic dark matter from $3.7 \times 10^{-2}\,\mathrm{GeV/cm^3}$ to $7.4 \times 10^{-2}\,\mathrm{GeV/cm^3}$ at Earth's position. The effect may even be symmetric as it subsides equally in both simulated directions with progressing distance from Earth. In contrast, figure 16 draws a rather blurred picture: asymmetric and with discernible effect only in one half of the galaxy. Nevertheless, a gravitational lensing effect is to be concluded for both figures, opposing a constant dark matter flux which in turn implies that galactic and extra galactic dark matter affect Milky Way's rotation curve. For this reason the measured dark matter from Milky Way's rotation curve is not solely made up of galactic dark matter. Both components' rotational velocity must be added up squarely to compensate for the missing luminous matter in Milky Way's rotation curve. Relation 29 shows any partial rotational velocity discernible in Milky Way's rotation curve caused by mass objects depends on the derivative of mass density. Until now neither the induced partial rotational velocity of galactic and extra galactic dark matter which corresponds to Milky Way's rotation curve nor their proportional contribution to Milky Way's rotation curve are known. Eventually the same quantity of extra galactic dark matter particles may account for a greater impact on Milky Way's rotation curve in contrast to galactic dark matter and vice versa. Indeed, the respective contributions of the same amount of dark matter particles seem to cause differing partial rotational velocities from each other by comparing the density profiles' slopes of galactic and extra galactic dark matter. For this reason galactic dark matter cannot simply be substituted by extra galactic dark matter as such the overall amount of dark matter determined from Milky Way's rotation curve is subject to change. Consequently the original and increased assessed extra galactic dark matter density does not necessarily equate to $\sim$ 12 % and $\sim$ 24 % of galactic dark matter respectively. Therefore, the galactic dark matter density is not to be determined and it is not possible to propose any quantitative or even qualitative estimate on the antimatter spectrum.

[5] Vectorial orientation needs to be considered.

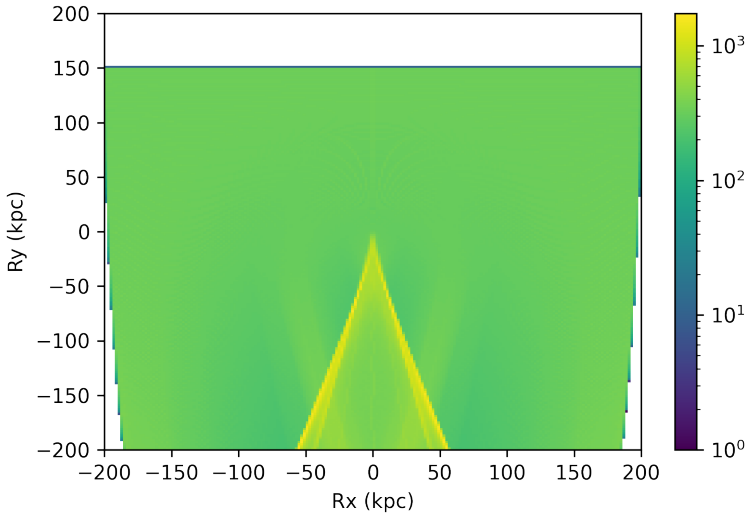

Figure 14: Simulated density distribution of an extra galactic dark matter flux in the Local Group's plane caused by the Milky Way's gravitational lensing effect

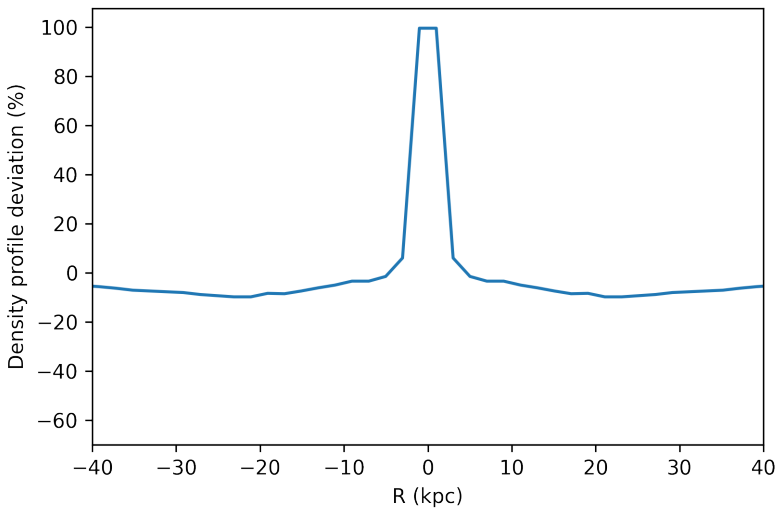

Figure 15: Simulated density deviation profile of an extra galactic dark matter flux along a horizontal axis $R_y = 8\,\mathrm{kpc}$ in the Local Group's plane caused by the Milky Way's gravitational lensing effect.

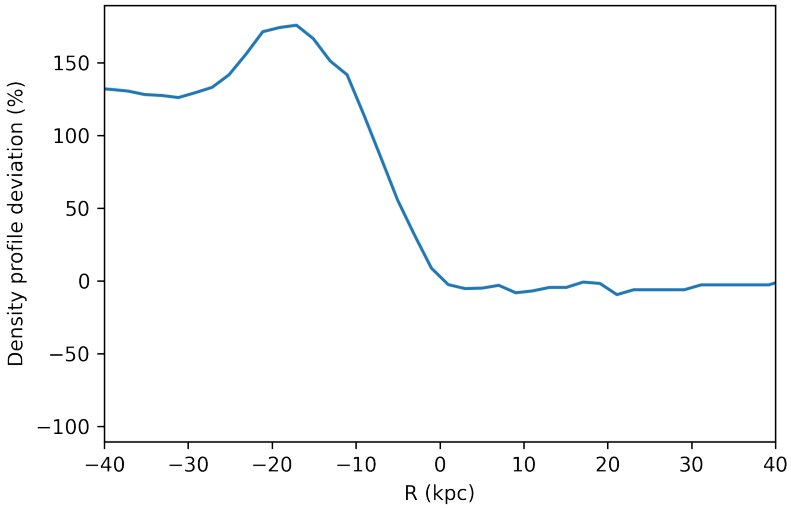

Figure 16: Simulated density deviation profile of an extra galactic dark matter flux along a vertical axis $R_x = 8\,\mathrm{kpc}$ in the Local Group's plane caused by the Milky Way's gravitational lensing effect

4.3 Velocity Dependent Effects on Antimatter's Creation from an Extra Galactic Dark Matter Flux

The assumption of extra galactic dark matter requires a speed above Milky Way's escape velocity, i.e. $|\mathbf{v}| \geq 600\,\mathrm{km\,s^{-1}}$. This fraction of dark matter does not annihilate itself in the center of mass frame in which measurements from Earth are mainly taken. Hence, the differential injection spectrum's reference frame needs to be shifted into the so called laboratory frame. For simplicity's sake the annihilation of two extra galactic dark matter particles is neglected. Assuming a dark matter annihilation between a galactic and an extra galactic dark matter particle with the latter being at Milky Way's escape velocity, the net velocity of both equal $300\,\mathrm{km\,s^{-1}}$ in their center of mass frame. Therefore, β and the Lorentz factor γ are calculated to equal 1×10^{-3} and $1{+}5 \times 10^{-7}$, respectively. Applying equation 21 and 23 the differential injection spectrum is shown in its laboratory frame in figure 17. For comparison purposes the differential injection spectrum is additionally plotted in the center of mass frame. The latter and the center of mass frame are found to be almost identical. Figure 18 depicts the exact ratio between laboratory frame and center of mass frame. The difference between both reference frames decreases with growing kinetic energy and speed respectively as it closes up on Milky Way's escape velocity. Consequently a maximum value of roughly 1.4 % is discernible for $T \lesssim 0.01\,\mathrm{GeV/A}$. Thus, the effect is negligible.

A further effect can be suspected in the cross section $< \sigma v >$ of equation 1. However, it is possible to use the expansion, equation 2. Plugging in the above calculated β of 1×10^{-3} shows p-wave annihilation is suppressed by a factor of 1×10^{-6} whereas s-wave annihilation is velocity independent. Thus, the effect is negligible as well.

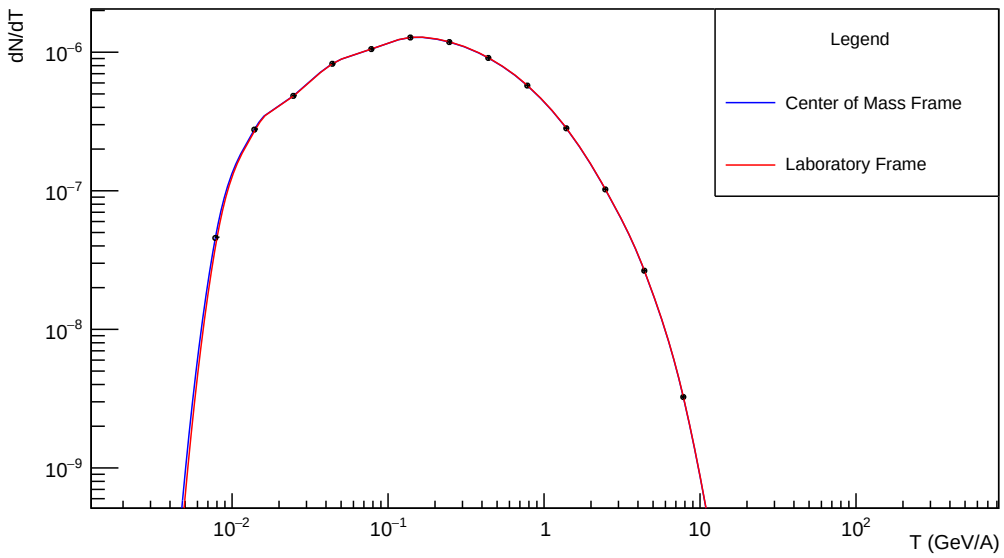

Figure 17: Differential injection spectrum plotted in the center of mass and laboratory frame

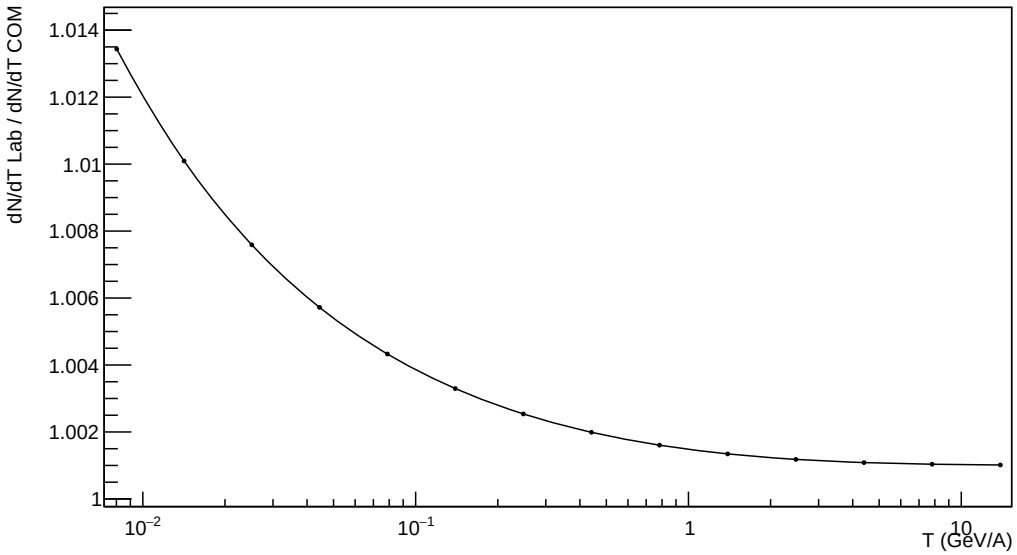

Figure 18: Ratio of differential injection spectrum laboratory frame over center of mass frame

5 Conclusion

Dark matter is a huge conundrum and much about it is still unknown. Actually the thesis opens more questions than it solves. As the sole dark matter existence is factually not proven the idea of an extra galactic dark matter flux is to be questioned even more. Eventually, the idea is still debated and calculation base on a toy model [2]. Additionally, a border of hydrogen which surrounds the Milky Way hindering extra galactic dark matter's particles to pass is not to be dismissed to current knowledge. Such a barrier could not only slow dark matter particles down, it may also significantly decrease the number of extra galactic particles. In fact, extra galactic dark matter's velocity is also uncertain due to two additional facts. Extra galactic dark matter's velocity must equal at least Milky Way's escape velocity; however the exact speed distribution is unknown. Moreover, assuming loose, homogeneously distributed dark matter particles within the Virgo Supercluster and consequently the Local Group Andromeda galaxy's escape velocity should be considered as well as it may differ from Milky Way's escape velocity, enhancing dark matter particle's speed. Therefore, the determined negligible effect on the cross section $< \sigma v >$ of a magnitude of $\sim 10^{-6}$ and the injection spectrum of 1.4 % should be considered under the caveat that extra galactic dark matter's speed cannot be ascertained.
Taking the existence of a dark matter flux for granted for the sake of this work other questions arise as well. Within the attempt to determine the dark matter density distribution from Milky Way's rotation curve the Milky Way is separated in its divisions and the partial caused rotational velocity of each component is calculated. Milky Way's rotation curve is primarily rebuilt without extra galactic dark matter and in the second stage a homogeneously distributed extra galactic dark matter flux is assumed. Within the rebuilt already, two minor ambiguities emerge to be released free for discussion. In some literature Milky Way's disc is separated into two parts which has been omitted in this thesis as laid out in the method in paper [1]. Difficulties in possible gains due to already overlapping functions and missing hints like peaks in Milky Way's rotation curve are speculated on. In figure 8 the result does no align with the one of paper [1].
According to a constant dark matter flux within the Milky Way a shifted Navarro-Frenk-White profile is proposed. Coherently, the profile does not approach point zero at any point so that no volume enclosing all dark matter particles can be chosen. For this reason the prerequisite for the use of Gauss's law for gravity is unmet. The failure is recognized by an increase of Milky Way's rotation curve beyond luminous matter where measurements request a flat rotation curve. Magnitude or direction of any physical object can only change if a net force is exerted. It is concluded that the force is proportional to the derivative of density. Hence, in line with measurements of Milky Way's rotation curve it should not be affected by a constant extra galactic dark matter flux. Nevertheless, it is discussed below that there is an impact on Milky Way's rotation curve from extra galactic dark matter due to a lensing effect contradicting a homogeneously distributed extra galactic dark matter flux. Therefore, the question remains how extra galactic dark matter's partial rotational velocity will be determined if Gauss's law for gravity is not applicable.
Moreover, the derived conclusion of the gravitational force being solely proportional to the derivative of dark matter's density instead of its original density may bother some. Eventually, this implies doubts on the applicability of Gauss's law for gravity on the original Navarro-Frenk-White profile. In fact, Gauss's law for gravity does not entail any derivative of mass density. As the discussed conclusion is a general statement for matter affected by gravity in such large scales this contradiction cannot be solved by specifying extra galactic dark matter only. Indeed, Gauss's law for gravity could be applied on spherical symmetric luminous matter as well and the inconsistency would still be present indissolubly.
Within a simulation on basic principles the Milky Way is modelled to function as a lens for extra galactic dark matter. One direction shows an increase of extra galactic dark matter density of 100 % at Earth's position. The result however should be verified within more dimensions and less simplifications. Three dimensions might be a riddle to solve as the rotation curve lies on the galactic plane and the gravitational force cannot be determined from Milky Way's rotation curve. Progress however requires a determination of the lensing effect on extra galactic dark matter as it affects galactic dark matter measurements from Milky Way's rotation curve indispensably. In fact, the overall amount of dark matter from Milky Way's rotation curve measurements varies for this reason. Hence, the dark matter distribution is unknown but as if this was not enough Gauss's law for gravity is not applicable and as such extra galactic dark matter's induced partial rotational velocity cannot be assessed. This is however crucial to determine the galactic dark matter density. Summing everything up: to current knowledge it is not even possible to estimate a qualitative outcome of the produced spectrum of antinuclei which in turn might be crucial to prove dark matter at all!

6 Acknowledgement

First of all, I would like to thank my supervisor M.Sc. Stephan Königstorfer for his constant support and his perpetual objective to enhance my knowledge and belief that I could be even better than what I have achieved so far. This thesis would not have been possible without you. Thank you!

I would like to thank M.Sc. Laura Serksnyte for her reasoning and distinict view on what Stephan Königstorfer and I might have overlooked, leading into engaging discussions advancing this thesis' content.
I would like to thank Prof. Dr. Alejandro Ibarra for his explanation on s-wave and p-wave annihihaltion. Moreover, my thanks goes to Mister Sofue et. al. who kindly provided me with the data points for the rotation curve.
Last but not least I would like to thank my professor Prof. Dr. Laura Fabbietti who allowed me to research an extra galactic dark matter flux and its expected consequences and supplying me with technical equipment.
But most of all I would like to thank the people around me who endured my grouch.

References

[1] Y. Sofue, "Rotation and mass in the Milky Way and spiral galaxies," *Publications of the Astronomical Society of Japan*, vol. 69, p. R1, Dec 2016.

[2] A. N. Baushev, "Extragalactic dark matter and direct detection experiments," *The Astrophysical Journal*, vol. 771, p. 117, Jun 2013.

[3] A. Cuoco, J. Heisig, L. Klamt, M. Korsmeier, and M. Krmer, "Scrutinizing the evidence for dark matter in cosmic-ray antiprotons," *Physical Review D*, vol. 99, May 2019.

[4] L. Baudis, "The search for dark matter," *European Review*, vol. 26, no. 1, pp. 70–81, 2018.

[5] K. Freese, "Status of dark matter in the universe," *International Journal of Modern Physics D*, vol. 26, p. 1730012, Mar 2017.

[6] D. Keeports, "Mass distributions implying flat galactic rotation curves," *European Journal of Physics*, vol. 31, p. 519, Mar 2010.

[7] V. A. Rubakov, "Cosmology and dark matter," 2019.

[8] J. E. Taylor, "Dark matter halos from the inside out," *Advances in Astronomy*, vol. 2011, pp. 1–17, 2011.

[9] V. Trimble, "Existence and nature of dark matter in the universe," *Annual Review of Astronomy and Astrophysics*, vol. 25, no. 1, pp. 425–472, 1987.

[10] P. v. Doetinchem, K. Perez, T. Aramaki, S. Baker, S. Barwick, R. Bird, M. Boezio, S. Boggs, M. Cui, A. Datta, and et al., "Cosmic-ray antinuclei as messengers of new physics: status and outlook for the new decade," *Journal of Cosmology and Astroparticle Physics*, vol. 2020, p. 035, Aug 2020.

[11] R. Bird, T. Aramaki, M. Boezio, S. E. Boggs, V. Bonvicini, D. Campana, W. W. Craig, E. Everson, L. Fabris, H. Fuke, F. Gahbauer, I. Garcia, C. Gerrity, C. J. Hailey, T. Hayashi, C. Kato, A. Kawachi, M. Kondo, M. Kozai, A. Lowell, M. Manghisoni, N. Marcelli, M. Martucci, S. I. Mognet, K. Munakata, R. Munini, S. Okazaki, J. Olson, R. A. Ong, G. Osteria, K. Perez, S. Quinn, V. Re, E. Riceputi, F. Rogers, J. L. Ryan, N. Saffold, V. Scotti, Y. Shimizu, R. Sparvoli, A. Stoessl, S. Takeuchi, E. Vannuccini, P. von Doetinchem, T. Wada, M. Xiao, A. Yoshida, T. Yoshida, G. Zampa, and J. Zweerink, "Gaps: Searching for dark matter using antinuclei in cosmic rays," 2019.

[12] S. M. Faber and J. S. Gallagher, "Masses and mass-to-light ratios of galaxies.," *Annual Review of Astronomy and Astrophysics*, vol. 17, pp. 135–187, Jan. 1979.

[13] J. Einasto, A. Kaasik, and E. Saar, "Dynamic evidence on massive coronas of galaxies," *Nature (London)*, vol. 250, pp. 309–310, Jul 1974.

[14] G. Chon, H. Bhringer, and S. Zaroubi, "On the definition of superclusters," *Astronomy Astrophysics*, vol. 575, p. L14, Mar 2015.

[15] E. J. Shaya, R. B. Tully, Y. Hoffman, and D. Pomarde, "Action dynamics of the local supercluster," *The Astrophysical Journal*, vol. 850, p. 207, Dec 2017.

[16] S. Bergh, p. 263. Cambridge Astrophysics, Cambridge University Press, 2000.

[17] M. M. Kachelrie, S. Ostapchenko, and J. Tjemsland, "Revisiting cosmic ray antinuclei fluxes with a new coalescence model," *Journal of Cosmology and Astroparticle Physics*, vol. 2020, p. 048048, Aug 2020.

[18] A. Arbey and F. Mahmoudi, "Dark matter and the early universe: A review," *Progress in Particle and Nuclear Physics*, p. 103865, Apr 2021.

[19] A. Cuoco, M. Krmer, and M. Korsmeier, "Novel dark matter constraints from antiprotons in light of ams-02," *Physical Review Letters*, vol. 118, May 2017.

[20] J. Herms, A. Ibarra, A. Vittino, and S. Wild, "Antideuterons in cosmic rays: sources and discovery potential," *Journal of Cosmology and Astroparticle Physics*, vol. 2017, p. 018, Feb 2017.

[21] T. R. Slatyer, "Les houches lectures on indirect detection of dark matter," 2021.

[22] A. Coogan and S. Profumo, "Origin of the tentative ams antihelium events," *Physical Review D*, vol. 96, Oct 2017.

[23] A. Coogan and S. Profumo, "Origin of the tentative ams antihelium events," *Physical Review D*, vol. 96, Oct 2017.

[24] A. Ibarra and S. Wild, "Prospects of antideuteron detection from dark matter annihilations or decays at ams-02 and gaps," *Journal of Cosmology and Astroparticle Physics*, vol. 2013, p. 021, Feb 2013.

[25] A. Das and B. Dasgupta, "Selection rule for enhanced dark matter annihilation," *Physical Review Letters*, vol. 118, Jun 2017.

[26] J. Lopes and I. Lopes, "New limits on thermally annihilating dark matter from neutrino telescopes," *The Astrophysical Journal*, vol. 827, p. 130, Aug 2016.

[27] Y. Sofue, "Rotation curve of the milky way and the dark matter density," 2020.

[28] K. Boshkayev and D. Malafarina, "A model for a dark matter core at the galactic centre," *Monthly Notices of the Royal Astronomical Society*, vol. 484, pp. 3325–3333, Jan 2019.

[29] Y. Sofue, "Rotation curve and mass distribution in the galactic center from black hole to entire galaxy," *Publications of the Astronomical Society of Japan*, vol. 65, p. 118, Dec 2013.

[30] F. R. S. Madrid, "On the age of the milky way bulge stellar population," September 2018.

[31] W. J. Maciel, *Astrophysics of the interstellar medium*, p. 115. Springer, 2013.

[32] J. M. VanDerHulst, *The interstellar medium in Galaxies*, pp. 75–103. Kluwer, 1997.

[33] M. Andre and A. Joao, *Star clusters in the era of large surveys proceedings of symposium 5 of Jenam 2010*, pp. 199–206,. Springer Berlin Heidelberg, 2012.

[34] G. Gilmore and N. Reid, "New light on faint stars III. Galactic structure towards the South Pole and the Galactic thick disc," *Monthly Notices of the Royal Astronomical Society*, vol. 202, pp. 1025–1047, 04 1983.

[35] R. P. Olling and M. R. Merrifield, "Two measures of the shape of the dark halo of the milky way," *Monthly Notices of the Royal Astronomical Society*, vol. 311, pp. 361–369, Jan 2000.

[36] R. W. Kühne, "Derivation of the Local Lorentz Gauge Transformation of a Dirac Spinor Field in Quantum Einstein-Cartan Theory." working paper or preprint, Nov. 2018.